Journal of the Meteorological Society of Japan

EARLY ONLINE RELEASE

The DOI for this manuscript is
DOI:10.2151/jmsj.2023-014
J-STAGE Advance published date: March 16th, 2023
The final manuscript after publication will replace the preliminary version at the above DOI once it is available.

Systematic global evaluation of seasonal climate forecast skill for monthly precipitation of JMA/MRI-CPS2 compared with a statistical forecast system using climate indices

Yuji MASUTOMI[1]

Center for Climate Change Adaptation, National Institute for Environmental Studies, 16-2 Onogawa, Tsukuba, Ibaraki 305-8506, Japan

Toshichika IIZUMI

Institute for Agro-Environmental Sciences, National Agriculture and Food Research Organization, 3-1-3 Kannondai, Tsukuba, Ibaraki 305-8604, Japan

Kei OYOSHI

Earth Observation Research Center, Japan Aerospace Exploration Agency, 2-1-1 Sengen, Tsukuba, Ibaraki 305-8505, Japan

Nobuyuki KAYABA

Japan Meteorological Agency, 3-6-9 Toranomon, Minato City, Tokyo 105-8431, Japan

Wonsik KIM

Institute for Agro-Environmental Sciences, National Agriculture and Food Research Organization, 3-1-3 Kannondai, Tsukuba, Ibaraki 305-8604, Japan

Takahiro TAKIMOTO

Institute for Agro-Environmental Sciences, National Agriculture and Food Research Organization, 3-1-3 Kannondai, Tsukuba, Ibaraki 305-8604, Japan

and

Yoshimitsu MASAKI

Institute for Agro-Environmental Sciences, National Agriculture and Food Research Organization, 3-1-3 Kannondai, Tsukuba, Ibaraki 305-8604, Japan

March 18, 2022

----

1) Corresponding author: Yuji Masutomi, Center for Climate Change Adaptation, National Institute for Environmental Studies, 16-2 Onogawa, Tsukuba, Ibaraki 305-8506, Japan.
Email: masutomi.yuji@nies.go.jp
Tel: +81-29-850-2438

Abstract

In this study, we aimed to systematically and globally evaluate the monthly precipitation forecasts of JMA/MRI-CPS2, a dynamical seasonal climate forecast (Dyn-SCF) system operated by the Japan Meteorological Agency, by comparing its forecasts with those of a statistical SCF (St-SCF) system using climate indices. We developed a new global St-SCF system using 17 climate indices and compared the monthly precipitation of this system with those of JMA/MRI-CPS2. Consequently, the skill of JMA/MRI-CPS2 was determined to be globally higher than that of the St-SCF for zero-month lead forecasts. In contrast, for forecasts made with one month or longer lead times, the deterministic skill of JMA/MRI-CPS2 was comparable to that of the St-SCF and the probabilistic skill of JMA/MRI-CPS2 remained slightly higher. In addition to evaluating the skill of JMA/MRI-CPS2, we identified several regions and seasons, for which JMA/MRI-CPS2 showed a low forecast skill, compared with the St-SCF. This indicated that JMA/MRI-CPS2 cannot adequately reproduce certain dynamics. In conclusion, comparing Dyn-SCFs with St-SCFs can clarify the potential regions and seasons to improve the forecast skill of Dyn-SCFs.

Keywords: seasonal climate forecast; JMA/MRI-CPS2; precipitation; climate index; forecast skill

1. Introduction

Seasonal climate forecasts (SCF), which are capable of making weather predictions with one month to one year lead times, provide useful information for decision-making and early warning systems in various fields such as agriculture and water resource management (Doblas-Reyes et al., 2006; Jones et al., 2000; Klemm and McPherson, 2017; Meinke and Stone, 2005; Pozzi et al., 2013); however, their utility relies on forecast skill. Therefore, SCF skill evaluation is crucial in the construction of SCF systems (Kim et al., 2012).

Generally, evaluating the skill of SCFs involves analyzing their degree of similarity with observed data. As a more advanced approach, using climatology or simple statistical methods in the assessment of added values compared to the SCF system has been proposed (Luo et al. 2012; Pappenberger et al. 2015; Turco et al. 2017). For dynamical SCF (Dyn-SCF) systems, particularly those with large computational loads, the benefits of these added values outweigh their high cost compared with the forecast skill of less expensive and simpler methods.

In the case of forecasting a few specific climate variables, statistical SCF (St-SCF) systems are an alternative to the Dyn-SCF systems (Doblas-Reyes et al., 2013). The forecast skills of the two systems have been compared in various manners and regions (Folland et al. 1991; Anderson et al. 1999; Barnston et al. 1999; van Oldenborgh et al. 2005; Quan et al. 2006; Wu et al. 2009; Pappenberger et al. 2015; Turco et al. 2017;

Lenssen et al. 2020). Systematic global comparisons can be used to identify the regions and seasons in which Dyn-SCF systems have advantages and disadvantages in forecasting.

Among the various statistical methods used in St-SCF systems, numerous studies have used climate indices such as Niño 3.4, the Southern Oscillation Index, and the Madden-Julian Oscillation (Quayle 1929; Nicholls, McBride, and Ormerod 1982; McBride and Nicholls 1983; Gordon 1986; Chu 1989; Stone, Hammer, and Marcussen 1996; Chiew et al. 1998; Kirono, Chiew, and Kent 2010; Schepen, Wang, and Robertson 2012; Eden et al. 2015; Singh and Qin 2020). The predictability in using climate indices relies on the slow dynamics of the ocean and atmosphere and their associated climate states. This is similar for Dyn-SCF systems, whose predictability also depends on the presence of slow variations in soil moisture, snow cover, sea ice, and ocean surface temperature (Doblas-Reyes et al., 2013). Therefore, the forecast skill of St-SCFs that utilize climate indices is a suitable benchmark for Dyn-SCFs. By comparing Dyn-SCFs and St-SCFs, slow dynamics, which are insufficiently reproduced in Dyn-SCF systems, can be clarified, contributing to improving the skill of Dyn-SCFs.

The global Dyn-SCF system known as JMA/MRI-CPS2 (Japan Meteorological Agency/Meteorological Research Institute-Coupled Prediction System version 2) (Takaya et al. 2018) developed by the Japan Meteorological Agency (JMA) and Meteorological Research Institute (MRI) is used for operational seasonal forecasting in Japan. Takaya et al. (2018) reported that JMA/MRI-CPS2 exhibited improved forecast skill performance on interannual variability in the ocean and atmosphere, including El Niño events, compared to its predecessor model, JMA/MRI-CPS1 (Takaya et al., 2017). The Tokyo Climate Center of the World Meteorological Organization publishes monthly forecast skills of JMA/MRI-CPS2. Their evaluation includes reports on where and when precipitation forecast skill is high or low. Currently, comparisons with St-SCFs have not been performed for JMA/MRI-CPS2.

Precipitation forecasting is essential for effective water management and disaster reduction. The precipitation forecast skill of Dyn-SCF systems is shown to be lower than that of temperature forecasts, and areas with highly accurate precipitation forecasts are limited in the tropics (Doblas-Reyes et al., 2013). To date, the added value of the skill of Dyn-SCF systems for precipitation forecasts compared to St-SCF systems has not been determined.

In this study, we aimed to evaluate the monthly precipitation forecast skill of JMA/MRI-CPS2 compared with that of an St-SCF system by using climate indices and discussed its likelihood of improving the forecast skill of Dyn-SCFs. The outline of this paper is as follows. Section 2 describes the data and methods, explaining the precipitation observation data (Section 2.1), the two models: JMA/MRI-CPS2 (Section 2.2) and an St-SCF using climate indices (Section 2.3), and the evaluation method of forecast skill (Section 2.4). Section 3 presents the results of forecast skill from three viewpoints: global (Section 3.1), spatial (Section 3.2), and regional (Section 3.3). Section 4 outlines and discusses the main findings. Finally, Section 5 gives the conclusions.

2. Data and methods

The forecast skill of JMA/MRI-CPS2 was evaluated by comparing it with observed precipitation. An St-SCF system that utilized 17 climate indices was then developed to generate monthly precipitation forecasts. The forecast skill of this St-SCF system was evaluated and compared to that of JMA/MRI-CPS2. Table 1 lists the data and models, as well as the method used for evaluating forecast skill.

2.1. Observation data on precipitation

Monthly precipitation data from the Global Precipitation Climatology Project (GPCP) (Adler et al., 2003, 2018) v2.3 provided by the Physical Sciences Laboratory of the National Oceanic & Atmospheric Administration/Office of Air and Radiation/Earth System Research Laboratories (NOAA/OAR/ESRL) were used as observations. Data from 1981 to 2020 was first divided into two half periods: 1981–2000 and 2001–2020. The data in the first period was used for the bias-correction of JMA/MRI-CPS2 (Section 2.2) and model development of the St-SCF system using climate indices (Section 2.3), and the second half period data was used for the evaluation of forecast skill of the two models (Section 2.4). As a pre-processing step, GPCP v2.3 was re-gridded to follow JMR/MRI-CPS2 using the bilinear method, because the center of their grids did not match even though the spatial resolution of both JMA/MRI-CPS2 and GPCP v2.3 was 2.5° × 2.5°.

2.2. JMA/MRI-CPS2

The main component of JMA/MRI-CPS2 is a coupled atmosphere–ocean model (JMA/MRI-CGCM2), with an atmospheric component based on the low-resolution version of the JMA Global Spectral Model (GMS1011C, Japan Meteorological Agency, 2013). Its spatial resolution is TL159 (approximately 110 km) with 60 vertical layers. The ocean component of JMA/MRI-CGCM2 is based on the MRI Community Ocean Model version 3 (Tsujino et al., 2010), which includes a sea ice model; it has a spatial resolution of 1° east–west and 0.3–0.5° north–south, and contains 52 vertical layers. The Japanese 55-year Reanalysis (Kobayashi et al. 2015) was used to initialize the atmospheric data, and the Global Ocean Data Assimilation System (MOVE/MRI.COM-G2 (Toyoda et al., 2013)) was used for ocean data.

The JMA/MRI-CPS2 hindcast data were obtained from the Japan Meteorological Business Support Center. The hindcast period was 1979–2020 and the time resolution was daily. Daily values were averaged to produce monthly values. The hindcast data had a spatial resolution of 2.5° × 2.5° and included five ensembles with different initial conditions, explained as follows. Two forecasts started near the middle and end of each month; this study used the forecast closer to the end of the month, with the dates: Jan 31, Feb 25, Mar 27, Apr 26, May 31, Jun 30, Jul 30, Aug 29, Sep 28, Oct 28, Nov 27, and Dec 27. The forecast values in the first six months of the hindcast data, which covered 240 days, was used in the study. Figure 1 shows an example of five-month lead forecasts of

JMA/MRI-CPS2. For example, precipitation forecasts for July used monthly precipitation forecasts that began in January.

The hindcast data for 2001–2020 was used for the evaluation of the forecast skill of JMA/MRI-CPS2. Before the evaluation, the data was bias-corrected, as follows:

$$\widetilde{SIM_{\imath,k,LM}}(Y,M) = SIM_{i,k,LM}(Y,M) + \left(\overline{OBS_{\imath}(M)} - \overline{SIM_{\imath,LM}(M)}\right)$$

$$\overline{OBS_{\imath}(M)} = \sum_{Y_{BC}=1981}^{2000} OBS_{i}(Y_{BC},M)$$

$$\overline{SIM_{\imath,LM}(M)} = \sum_{k=1}^{5}\sum_{Y_{BC}=1981}^{2000} SIM_{i,k,LM}(Y_{BC},M)$$

where $\widetilde{SIM_{\imath,k}(Y,M)}$ denotes bias-corrected forecast values for grid *i*, ensemble *k* (= 1 to 5), lead month *LM* (= 0 to 5) for forecast year *Y* (= 2001 to 2020), and month *M*. $\overline{OBS_{\imath}(M)}$ is the observed precipitation averaged over the years for bias-correction, Y_{BC} (= 1981 to 2000), for grid *i* and month *M*, and $\overline{SIM_{\imath,LM}(M)}$ are forecasted precipitation averaged over the years for bias-correction (Y_{BC} = 1981 to 2000) and ensembles (*k* = 1 to 5) for grid *i* and lead month *LM*.

2.3. Statistical seasonal climate forecast system using climate indices

The St-SCF system using climate indices was constructed by first producing 17 precipitation forecasts from 1981 to 2000 with statistical models for the 17 climate indices. Second, the statistical model for the climate index with the highest Mean Squared Skill Score (MSSS) was selected. Third, 100 ensembles of the statistical model for the climate index were produced by the resampling method. Fourth, 100 ensembles of precipitation forecasts from 2001 to 2020 were produced by using the 100 ensembles of the statistical model.

Statistical models used in this study treat the climate index as the explanatory variable and precipitation as the objective variable. The model is expressed as follows:

$$PRE_{i,j,LM}(Y,M) = \max\{f_{i,j,M,LM}(IDX_j(Y, M-(LM+1))),0\}$$

where $PRE_{i,j,LM}(Y,M)$ denotes the forecast values of precipitation for grid *i*, climatic index *j*, lead month *LM* (= 0 to 5), forecast year *Y,* and month *M*. The expression $IDX_j(M-(LM+1))$ is the value of climatic index *j* in *M* – (*LM* + 1), and $f_{i,j,M,LM}$ is a function for the precipitation in *M* for grid *i* from climatic index *j* in *M* – (*LM* + 1). Figure 1 shows an example of a five-month lead forecast by the St-SCF using climate indices. In the statistical model for precipitation forecasts in July, the precipitation for that month was treated as the objective variable and the climate indices in January as the explanatory variables.

In the first step, the leave-one-out method was used for producing precipitation forecasts from 1981 to 2000. After removing the data of one forecast year from 1981 to 2000, the function $f_{i,j,M,LM}$ was determined by using the remaining data through the smoothing spline method (Wood, 2017). In this study, the “gam” function in the “mgcv” package of R software v4.05 was used for the smoothing spline method. An example of this function, $f_{i,j,M,LM}$, is shown in Figure 2. Next, the forecast values were obtained using the function determined from $f_{i,j,M,LM}$ and the data removed in the first step. By repeating the above procedures for all years from 1981 to 2000, forecast values were obtained. In addition to the smoothing spline method, linear models were also used for the function, $f_{i,j,M,LM}$. The description of a part of the forecast skill of the linear models has been provided as Appendix.

In the third step, 100 ensembles of the statistical model for the climate index with the highest MSSS were constructed with the resampling method (Eflon, 1979; Masutomi et al., 2012; Masutomi et al., 2015). First, $f_{i,j,M,LM}$ was determined by using the statistical model for the climate index with the highest MSSS and precipitation data from 1981 to 2000 with the smoothing spline method. Note that the leave-one-out method was not used in this step. Then, new precipitation data from 1981 to 2000 were produced by resampling residues between observed precipitation and precipitation calculated by the determined $f_{i,j,M,LM}$ and by adding the resampled residues to the observed precipitation. By repeating the resampling procedures 100 times, 100 ensembles of new precipitation data were obtained. In the final step, 100 ensembles of $f_{i,j,M,LM}$ were constructed by the 100 ensembles of new precipitation data through the smoothing spline method.

Table 2 summarizes the 17 climate indices used in this study by category. These indices were selected from climate indices provided by the NOAA Physical Sciences Laboratory, and the values were updated within approximately a week after the end of each month.

2.4. Evaluation of forecast skill

The deterministic and probabilistic forecast skills of JMA/MRI-CPS2 and St-SCF using climate indices were evaluated. The MSSS was used for the deterministic forecast skill, while the area under receiver operating characteristic curve (AUC) was used for the probabilistic one. The MSSS value is expressed as:

$$MSSS(M) = 1 - \frac{MSE(M)}{VAR(M)},$$

$$MSE(M) = \frac{1}{N}\sum_{Y=2001}^{2020}\big(F(Y,M) - O(Y,M)\big)^2,$$

$$VAR(M) = \frac{1}{N}\sum_{Y=2001}^{2020}(O(Y,M) - \bar{O}(M))^2,$$

where $MSE(M)$ is the mean squared error for month *M*, $VAR(M)$ is the variance for month *M*, $F(Y,M)$ and $O(Y,M)$ are, respectively, forecast and observation values in year *Y* (= 2001 to 2020), *N* (= 20) is the number of years for the evaluation, and $\bar{O}(M)$ is mean precipitation over 20 years from 2001 to 2020 for month *M*. A positive MSSS value indicates that the forecast has higher skill than climatological forecasts. For the evaluation of deterministic forecast skill, five ensemble mean values of JMA/MRI-CPS2 and 100 of the St-SCF using climate indices were used.

The AUC was calculated above and below the mean observational precipitation during 2001−2020. The forecast probability for each category was calculated using the ensembles of each model. The mean value of AUCs for each category was used for the evaluation. The detailed calculation of the AUC is described in Mason (2018). An AUC is smaller than 0.5 means that the forecast skill is lower than that of climatological forecasts.

The evaluation was conducted for global data at a spatial resolution of 2.5° × 2.5° for JMA/MRI-CPS2 and the St-SCF system using climate indices. In addition to the global evaluation by grids, the following five global metrics were calculated: (i) MSSS-rp: the ratio of areas with positive MSSS; (ii) MSSS-hi: the ratio of areas with positive and higher MSSS between JMA/MRI-CPS2 and the St-SCF using climate indices; (iii) AUC-av: the global average of AUC; (iv) AUC-r0.5: the ratio of areas with AUC >0.5; (v) AUC-hi: the ratio of areas with AUC >0.5 and the higher AUC between JMA/MRI-CPS2 and St-SCF using climate indices. The calculations of these metrics are described in Figure 3. AUC-av is a simple metric for representing the global average AUC. While the global average of MSSS (MSSS-av) can be calculated, it was not used in this study because MSSS has no lower limit. Moreover, large MSSS negative values in any grid tend to influence the global mean. MSSS-rp and AUC-r0.5 are used to represent the ratio of areas where models have higher forecast skill than climatology or random forecasts, respectively. MSSS-hi and AUC-hi are the metrics for representing the ratio of areas with higher forecast skill and are appropriate for understanding the improved model. Note that all values of forecast skill are shown with three significant digits, although the significant digits of the original data are unknown.

3. Results

3.1. Comparison of global forecast skill

Figure 4 shows the global values of MSSS-rp and AUC-av for JMA/MRI-CPS2 for each lead month. Although JMA/MRI-CPS2 has high forecast skill in zero-month lead forecasts, the forecast skill decreases rapidly in the one-month lead forecasts, and gradually declines thereafter. The highest forecast skill of zero-month lead forecasts was observed in February, with an MSSS-rp of 0.325 and AUC-av of 0.643, while the worst forecast skill was observed in two different months: May with an MSSS-rp of 0.213, and September with an AUC-av of 0.590. For one-month lead forecasts, February had an MSSS-rp of 0.157, less than half the value of zero-month lead forecasts. Comparing the MSSS-rp and AUC-av of the ocean and land, the forecast skill for ocean is evidently higher than that for land.

Figure 5 shows the global values of MSSS-rp and AUC-av for the St-SCF using climate indices for each lead month. The forecast skill decreases as the lead month increases, but the decrease is significantly smaller than in JMA/MRI-CPS2. The highest forecast skill of zero-month lead forecasts for the global forecast was observed in two months: December with an MSSS-rp of 0.172, and January with an AUC-av of 0.537, while the worst forecast skill was observed in: April with an MSSS-rp of 0.136, and June with an AUC-av of 0.513. For one-month and five-month lead forecasts, the MSSS-rps of December were 0.157 and 0.145, and the AUC-avs of January were 0.532 and 0.521, respectively. Comparing the ocean and land areas shows that the forecast skill is higher for ocean forecasts with lead times of zero to five months.

Figure 6 shows a comparison of the annual mean deterministic (MSSS-rp, MSSS-hi) and probabilistic (AUC-av, AUC-r0.5, and AUC-hi) forecast skills between JMA/MRI-CPS2 and the St-SCF using climate indices. Evidently, both the deterministic and probabilistic forecast skills of JMA/MRI-CPS2 were much higher than those of the St-SCF for zero-month lead time. The difference drastically became smaller for one-month leads. For one-month or longer lead forecasts, deterministic forecast skills (MSSS-rp, MSSS-hi) between JMA/MRI-CPS2 and the St-SCF using climate indices were not different. The probabilistic forecast skills (AUC-av, AUC-r0.5, and AUC-hi) of JMA/MRI-CPS2 were still higher than that of the St-SCF using climate indices, although the difference was small and gradually decreased for longer lead forecasts. Therefore, the forecast skill of JMA/MRI-CPS2 is generally higher for zero-month lead forecasts. However, if the forecasts are longer than one month, the deterministic skill of JMA/MRI-CPS2 is comparable to that of the St-SCF using climate indices while the probabilistic skill of JMA/MRI-CPS2 remains slightly higher.

3.2. Spatial comparison of global forecast skill

Figure 7 shows the spatial distribution of MSSS for JMA/MRI-CPS2 in March, June, September, and December. In zero-month lead forecasts, areas with a positive MSSS is distributed worldwide; even in the middle latitudes, such as east Australia in September and Kazakhstan in December. However, the areas with positive MSSS were limited to low latitudes in one-month or longer lead forecasts.

Figure 8 shows the spatial distribution of MSSS for the St-SCF using climate indices for the same months as shown in Figure 7. The figure shows that the areas with high MSSS are generally limited to low latitudes even in zero-month lead forecasts. Figure 9 shows the climate indices selected for each grid with positive MSSS, demonstrating that the selected indices depend on the regions and forecast month. Table 3 presents the area ratio of selected climate indices for one-month lead forecasts. The climate index with the largest selected area was MEI. The indices whose ratio of the selected area is >0.01 were MEI, NINO1.2, NINO3, NINO3.4, NINO4, and SOI, which are ENSO-related, indicating that the St-SCF using climate indices largely relied on ENSO, presenting a physical background of the model.

Figure 10 shows the annual mean of MSSS-hi (left) and AUC-hi (right) by latitudes for JMA/MRI-CPS2 (red line) and the St-SCF using climate indices (black line). The deterministic and probabilistic forecast skills of JMA/MRI-CPS2 were generally higher than those of the St-SCF using climate indices at all latitudes for zero-month lead forecasts. For one-month or longer lead forecasts, the skills of JMA/MRI-CPS2 were still higher than those of the St-SCF using climate indices at low latitudes, but as the lead month increases, the differences between the two models decreased and the latitudes at which JMA/MRI-CPS2 has a higher forecast skill tended to narrow. Comparing the probabilistic and deterministic forecasts, the differences in probabilistic forecasts between JMA/MRI-CPS2 and the St-SCF using climate indices were larger at low latitudes than those in the deterministic forecasts. This is because the AUC-hi of the JMA/MRI-CPS2 at low latitudes was higher than that at high latitudes, while the AUC-hi of the St-SCF using climate indices did not change by latitudes. This is the reason why the global probabilistic forecast skills of JMA/MRI-CPS2 were slightly higher than those of the St-SCF using climate indices for one-month or longer lead forecasts, while there were no differences in the global deterministic forecasts between the two models (Figure 6).

3.3. Regional comparison of forecast skill for south Philippines in April and southwest Australia in December

Figures 7 and 8 show that the St-SCF using climate indices have a positive MSSS in south Philippines during April and southwest Australia during December from zero- to two-month lead forecasts; JMA/MRI-CPS2 had a negative MSSS. Figure 11 compares the precipitation at a grid in south Philippines (a; 120º E, 10º N) for April and in southwest Australia (b; 117.5 º E and 30º S) for December from 2001 to 2020 between observations and forecasts for zero- to two-month lead times by JMA/MRI-CPS2 and the St-SCF using climate indices. The MSSS values are also shown in Figure 11. The MSSSs of the St-SCF using climate indices were positive and higher than those by JMA/MRI-CPS2. In particular, they could accurately reproduce the annual variation of observations, even for forecasts two months in advance; whereas JMA/MRI-CPS2 was unable to forecast them. Figure 12 shows the relationship between climate indices and precipitation based on observations and forecasts of JMA/MRI-CPS2 for south Philippines and southwest Australia. From this figure, the inadequacies of the forecasts of JMA/MRI-CPS2 are evident. For example, in the zero-month-led forecasts of JMA/MRI-CPS2 for south Philippines, the linear relationship between climate indices and the forecasted precipitation was weak, with the forecasted precipitation showing a larger variation than the observation precipitation, especially for indices in the range –1 to 0. Although the forecasts of JMA/MRI-CPS2 with one- and two-month lead times showed a clear linear relationship with the climate indices, they tended to overestimate precipitation in south Philippines. Additionally, the forecasts for Australia could not reproduce higher precipitation for large negative indices, i.e., below –1; at an index of approximately 0, the zero-month led forecasts of JMA/MRI-CPS2 were associated with a large error. These results indicated that certain dynamics were not well reproduced by JMA/MRI-CPS2, implying that further analysis and incorporation of these dynamics into this forecast system will improve its forecast skill.

4. Discussion

4.1. Forecast skill of JMA/MRI-CPS2 in comparison to St-SCF

The forecast skill of JMA/MRI-CPS2 was evaluated by Takaya et al. (2018) and published by the Tokyo Climate Center. That evaluation showed that the forecast skill of precipitation was higher at low latitudes and for zero-month lead forecasts; MSSS, the deterministic forecast skill, is highest in February and lowest in April to June, while AUC, the probabilistic skill, is highest in February and lowest in September. The same forecast skills were confirmed in this study (Figures 4 and 7). In addition, by comparing with the St-SCF using climate indices as benchmark, we identified the regions and lead periods in which JMA/MRI-CPS2 was advantageous. For example, the zero-month lead forecast skill of JMA/MRI-CPS2 was globally higher than that of the St-SCF (Figures 6 and 10). In general, Dyn-SCF systems are known to have particularly high forecast skill in the tropics (Doblas-Reyes et al., 2013). Our study is the first to demonstrate the added value of Dyn-SCF systems on one-month lead forecasts over St-SCF systems. Additionally, for forecasts longer than a month, the deterministic skill of JMA/MRI-CPS2 was comparable to that of the St-SCF using climate indices and the probabilistic skill of JMA/MRI-CPS2 was slightly higher (Figure 6). At mid- and high-latitudes, no large differences were observed in deterministic and probabilistic forecast skills between the two models (Figure 10). These results clearly indicate that improving the skill of JMA/MRI-CPS2 for longer-term forecasts over one month is a challenge that must be addressed. The improvement in the skill of Dyn-SCFs in comparison to St-SCFs is discussed in the next section.

4.2. Improvement of forecast skill by comparing with St-SCF using climate indices

Various methods have been proposed to improve the forecast skill of Dyn-SCFs, including the initialization of soil moisture (Prodhomme et al., 2016b) and higher resolution (Prodhomme et al., 2016a). For JMA/MRI-CPS2, Takaya et al. (2021) showed that the forecast skill increases significantly with the number of ensembles. However, the realization of these improvements required a great deal of effort. In addition, if potential regions and seasons for improvement were known in advance, the model improvement could have been more efficient. In this study, by comparing the forecast skill of JMA/MRI-CPS2 with that of the St-SCF system, we found that in several regions and seasons, JMA/MRI-CPS2 showed a low forecast skill whereas the St-SCF using climate indices showed a high forecast skill. This clearly indicated the presence of certain dynamics that are not well-reproduced by JMA/MRI-CPS2, implying that the skill of the Dyn-SCF system could still be improved via the incorporation of these dynamics. Therefore, the comparison between them clearly highlights potential regions and seasons for improvement of forecast skill. Thus, we proposed an approach for identifying such regions and seasons by comparing the forecast skill of Dyn-SCFs with that of St-SCFs.

5. Conclusions

By comparing JMA/MRI-CPS2 with an St-SCF using climate indices as a benchmark, we identified the regions and lead periods in which JMA/MRI-CPS2 performed better. The main findings are as follows:

(i): The skill of JMA/MRI-CPS2 for global zero-month lead forecasts was higher than that of the St-SCF.

(ii): For one-month or longer forecasts, the deterministic skill of JMA/MRI-CPS2 was comparable to that of the St-SCF and its probabilistic skill was slightly higher.

These findings not only present the significant added value of JMA/MRI-CPS2, but also its challenges for model improvement. In addition, the comparison of JMA/MRI-CPS2 and the St-SCF using climate indices identified the potential regions and seasons for which JMA/MRI-CPS2 does not adequately reproduce climate dynamics, implying that the skill of Dyn-SCFs can still be improved by incorporating these dynamics into the Dyn-SCF system. Thus, we concluded that:

(iii) Comparing Dyn-SCFs with St-SCFs can determine potential regions and seasons for improvement of the forecast skill of Dyn-SCFs.

This approach is expected to be widely applied to improve the forecast skill of Dyn-SCFs.

Acknowledgments

This study was partly supported by the Coordination Fund for Promoting AeroSpace Utilization (JPJ000959) from the Ministry of Education, Culture, Sports, Science and Technology (MEXT), by KAKENHI (JP19H03069) from the Japan Society for the Promotion of Science (JSPS), and by the Climate Change Adaptation Research Program at National Institute for Environmental Studies.

Data availability

The JMA/MRI-CPS2 hindcast data can be purchased from the Japan Meteorological Business Support Center (http://www.jmbsc.or.jp/en/index-e.html). GPCP v2.3 is available at https://psl.noaa.gov/data/gridded/data.gpcp.html. The URLs where the 17 climate indices are obtained are listed in Table 2. All of the source codes used for the analyses in the present paper are stored at https://doi.org/10.5281/zenodo.5090304, while the source code of JMA/MRI-CPS2 is not opened for the public.

References

Adler, R. F., Huffman, G. J., Chang, A., Ferraro, R., Xie, P., Janowiak, J., Rudolf, B., Schneider, U., Curtis, S., Bolvin, D., Gruber, A., Susskind, J., Arkin, P. and Nelkin, E.: The version-2 global precipitation climatology project (GPCP) monthly precipitation analysis (1979–present) [online] Available from: https://journals.ametsoc.org/view/journals/hydr/4/6/1525-7541_2003_004_1147_tvgpcp_2_0_co_2.xml, J. Hydrometeor., 4(6), 1147–1167, 2003.

Adler, R. F., Sapiano, M., Huffman, G. J., Wang, J., Gu, G., Bolvin, D., Chiu, L., Schneider, U., Becker, A., Nelkin, E., Xie, P., Ferraro, R. and Shin, D. B.: The Global Precipitation Climatology Project (GPCP) monthly analysis (new version 2.3) and a review of 2017 global precipitation, Atmosphere (Basel), 9(4), doi:10.3390/atmos9040138, 2018.

Anderson, J., van den Dool, H., Barnston, A., Chen, W., Stern, W. and Ploshay, J.: Present-day capabilities of numerical and statistical models for atmospheric extratropical seasonal simulation and prediction, Bull. Am. Meteorol. Soc., 80(7), 1349–1361, 1999.

Barnston, A. G., He, Y. and Glantz, M. H.: Predictive skill of statistical and dynamical climate models in SST forecasts during the 1997–98 El Niño episode and the 1998 La Nina onset, Bull. Am. Meteorol. Soc., 80(2), 217–243, 1999.

Chiew, F. H. S., Piechota, T. C., Dracup, J. A. and McMahon, T. A.: El Nino/Southern Oscillation and Australian rainfall, streamflow and drought: Links and potential for forecasting, J. Hydrol., 204(1–4), 138–149, 1998.

Chu, P.-S.: Hawaiian drought and the southern oscillation, Int. J. Climatol., 9(6), 619–631, 1989.

Doblas-Reyes, F. J., Hagedorn, R. and Palmer, T. N.: Developments in dynamical seasonal forecasting relevant to agricultural management, Clim. Res., 33, 19–26, 2006.

Doblas-Reyes, F. J., García-Serrano, J., Lienert, F., Biescas, A. P. and Rodrigues, L. R. L.: Seasonal climate predictability and forecasting: Status and prospects, WIREs Clim. Change, 4(4), 245–268, 2013.

Eden, J. M., van Oldenborgh, G. J., Hawkins, E. and Suckling, E. B.: A global empirical system for probabilistic seasonal climate prediction, Geosci. Model Dev., 8(12), 3947–3973, 2015.

Efron, B.: Bootstrap methods: another look at the jackknife. Ann. Stat. 7, 1–26, 1979.

Folland, C., Owen, J., Ward, M. N. and Colman, A.: Prediction of seasonal rainfall in the Sahel region using empirical and dynamical methods, J. Forecast., 10(1–2), 21–56, 1991.

Gordon, N. D.: The southern oscillation and New Zealand weather, Mon. Wea. Rev., 114(2), 371–387, 1986.

Japan Meteorological Agency: Outline of the operational numerical weather prediction at the Japan Meteorological Agency [online] Available from: https://www.jma.go.jp/jma/jma-eng/jma-center/nwp/outline2013-nwp/pdf/outline2013_all.pdf, 2013.

Jones, J. W., Hansen, J. W., Royce, F. S. and Messina, C. D.: Potential benefits of climate forecasting to agriculture, Agric. Ecosyst. Environ., 82(1–3), 169–184, doi:10.1016/S0167-8809(00)00225-5, 2000.

Kim, H.-M., Webster, P. J. and Curry, J. A.: Seasonal prediction skill of ECMWF System 4 and NCEP CFSv2 retrospective forecast for the Northern Hemisphere Winter, Clim. Dyn., 39(12), 2957–2973, doi:10.1007/s00382-012-1364-6, 2012.

Kirono, D. G. C., Chiew, F. H. S. and Kent, D. M.: Identification of best predictors for forecasting seasonal rainfall and runoff in Australia, Hydrol. Processes, n/a–n/a, doi:10.1002/hyp.7585, 2010.

Klemm, T. and McPherson, R. A.: The development of seasonal climate forecasting for agricultural producers, Agric. For. Meteorol., 232, 384–399, 2017.

Kobayashi, S., Ota, Y., Harada, Y., Ebita, A., Moriya, M., Onoda, H., Onogi, K., Kamahori, H., Kobayashi, C., Endo, H., Miyaoka, K. and Takahashi, K.: The JRA-55 reanalysis: General specifications and basic characteristics, J. Meteorol. Soc. Jpn, 93(1), 5–48, 2015.

Lenssen, N., Goddard, L., and Mason, S.: Seasonal Forecast Skill of ENSO Teleconnection Maps, Weather and Forecasting, 35, 2387–2406, 2020.

Luo, Y. Q., Randerson, J. T., Abramowitz, G., Bacour, C., Blyth, E., Carvalhais, N., Ciais, P., Dalmonech, D., Fisher, J. B., Fisher, R., Friedlingstein, P., Hibbard, K., Hoffman, F., Huntzinger, D., Jones, C. D., Koven, C., Lawrence, D., Li, D. J., Mahecha, M., Niu, S. L., Norby, R., Piao, S. L., Qi, X., Peylin, P., Prentice, I. C., Riley, W., Reichstein, M., Schwalm, C., Wang, Y. P., Xia, J. Y., Zaehle, S. and Zhou, X. H.: A framework for benchmarking land models, Biogeosciences, 9(10), 3857–3874, 2012.

Mason, S. J.: Guidance on verification of operational seasonal climate forecasts, WMO, 2018.

Masutomi, Y., Iizumi, T., Takahashi, K. and Yokozawa, M.: Estimation of the damage area due to tropical cyclones using fragility curves for paddy rice in Japan. Environ. Res. Lett., 7, 014020, 2012.

Masutomi, Y., Arakawa, M., Minoda, T., Yonekura, T. and Shimada, T.: Critical air temperature and sensitivity of the incidence of chalky rice kernels for the rice cultivar ‘Sai-no-kagayaki’, Agric. For. Meteorol. 20311–16, 2015.

McBride, J. L. and Nicholls, N.: Seasonal relationships between Australian rainfall and the Southern Oscillation, Mon. Wea. Rev., 111(10), 1998–2004, 1983.

Meinke, H. and Stone, R. C.: Seasonal and inter-annual climate forecasting: The new tool for increasing preparedness to climate variability and change in agricultural planning and operations, Clim. Change, 70(1–2), 221–253, 2005.

Nicholls, N., McBride, J. L. and Ormerod, R. J.: On predicting the onset of the Australian wet season at Darwin, Mon, Mon. Wea. Rev., 110(1), 14–17, 1982.

Jan van Oldenborgh, G. J., Balmaseda, M. A., Ferranti, L., Stockdale, T. N. and Anderson, D. L. T.: Did the ECMWF seasonal forecast model outperform statistical ENSO forecast models over the last 15 years?, J. Clim., 18(16), 3240–3249, 2005.

Pappenberger, F., Ramos, M. H., Cloke, H. L., Wetterhall, F., Alfieri, L., Bogner, K., Mueller, A. and Salamon, P.: How do I know if my forecasts are better? Using benchmarks in hydrological ensemble prediction, J. Hydrol., 522, 697–713, 2015.

Pozzi, W., Sheffield, J., Stefanski, R., Cripe, D., Pulwarty, R., Vogt, J. V., Heim, R. R., Brewer, M. J., Svoboda, M., Westerhoff, R., van Dijk, A. I. J. M., Lloyd-Hughes, B., Pappenberger, F., Werner, M., Dutra, E., Wetterhall, F., Wagner, W., Schubert, S., Mo, K., Nicholson, M., Bettio, L., Nunez, L., van Beek, R., Bierkens, M., de Goncalves, L. G. G., de Mattos, J. G. Z. and Lawford, R.: Toward global drought early warning capability: Expanding international cooperation for the development of a framework for monitoring and forecasting, Bull. Am. Meteorol. Soc., 94(6), 776–785, 2013.

Prodhomme, C., Batté, L., Massonnet, F., Davini, P., Bellprat, O., Guemas, V. and Doblas-Reyes, F. J.: Benefits of increasing the model resolution for the seasonal forecast quality in EC-earth, J. Clim., 29(24), 9141–9162, 2016a.

Prodhomme, C., Doblas-Reyes, F., Bellprat, O. and Dutra, E.: Impact of land-surface initialization on sub-seasonal to seasonal forecasts over Europe, Clim. Dyn., 47(3–4), 919–935, 2016b.

Quan, X., Hoerling, M., Whitaker, J., Bates, G. and Xu, T.: Diagnosing sources of US seasonal forecast skill, J. Clim., 19(13), 3279–3293, 2006.

Quayle, E. T., Long-range rainfall forecasting from tropical (Darwin) air pressures. Royal Society of Victoria, 1929.

Schepen, A., Wang, Q. J. and Robertson, D.: Evidence for using lagged climate indices to forecast Australian seasonal rainfall, J. Clim., 25(4), 1230–1246, 2012.

Singh, V. and Qin, X.: Study of rainfall variabilities in Southeast Asia using long-term gridded rainfall and its substantiation through global climate indices, J. Hydrol., 585, 124320, 2020.

Stone, R. C., Hammer, G. L. and Marcussen, T.: Prediction of global rainfall probabilities using phases of the Southern Oscillation Index, Nature, 384(6606), 252–255, doi:10.1038/384252a0, 1996.

Takaya, Y., Yasuda, T., Fujii, Y., Matsumoto, S., Soga, T., Mori, H., Hirai, M., Ishikawa, I., Sato, H., Shimpo, A., Kamachi, M. and Ose, T.: Japan Meteorological Agency/Meteorological Research Institute-Coupled Prediction System version 1 (JMA/MRI-CPS1) for operational seasonal forecasting, Clim. Dyn., 48(1–2), 313–333, 2017.

Takaya, Y., Hirahara, S., Yasuda, T., Matsueda, S., Toyoda, T., Fujii, Y., Sugimoto, H., Matsukawa, C., Ishikawa, I., Mori, H., Nagasawa, R., Kubo, Y., Adachi, N., Yamanaka, G., Kuragano, T., Shimpo, A., Maeda, S. and Ose, T.: Japan Meteorological

Agency/Meteorological Research Institute-Coupled Prediction System version 2 (JMA/MRI-CPS2): Atmosphere–land–ocean–sea ice coupled prediction system for operational seasonal forecasting, Clim. Dyn., 50(3–4), 751–765, 2018.

Takaya, Y., Kosaka, Y., Watanabe, M. and Maeda, S.: Skilful predictions of the Asian summer monsoon one year ahead, Nat. Commun., 12(1), 2094, 2021.

Toyoda, T., Fujii, Y., Yasuda, T., Usui, N., Iwao, T., Kuragano, T. and Kamachi, M.: Improved analysis of seasonal-interannual fields using a global ocean data assimilation system, Theor. Appl. Mech. Jpn, 61, 31–48, 2013.

Tsujino, H., Motoi, T., Ishikawa, I., Hirabara, M., Nakano, H., Yamanaka, G., Yasuda, T., and Ishizaki, H.: Reference manual for the Meteorological Research Institute Community Ocean Model (MRI. COM) version 3, Meteorolog. Research Inst., 2010.

Turco, M., Ceglar, A., Prodhomme, C., Soret, A., Toreti, A. and Doblas-Reyes Francisco, J.: Summer drought predictability over Europe: Empirical versus dynamical forecasts, Environ. Res. Lett., 12(8), 084006, 2017.

Wu, Z., Wang, B., Li, J. and Jin, F.-F.: An empirical seasonal prediction model of the east Asian summer monsoon using ENSO and NAO, J. Geophys. Res., 114(D18), (D18), doi:10.1029/2009JD011733, 2009.

Wood, S.: Generalized additive models: An introduction with R, GAM computation vehicle with Automatic Smoothness estimation, Chapman and Hall/CRC, 2017.

Appendix

Figure A1 shows the MSSS-rp and MSSS-hi for JMA/MRI-CPS2 and the St-SCF using climate indices based on the spline method (St-SCF-spl) and St-SCF using climate indices based on the linear method (St-SCF-lin). No difference was detected in the forecast skill between St-SCF-spl and St-SCF-lin.

List of Figures

Figure 1: Five-month lead forecasts by JMA/MRI-CPS2 and the St-SCF using climate indices.

Figure 2: Spline interpolation curve (red line) of MEI in July for estimating August precipitation at 110º longitude and –2.5º latitude. The plots denote the observational precipitation and the values of the MEI.

Figure 3: Example calculations of (i) MSSS-rp: the ratio of areas with positive MSSS; (ii) MSSS-hi: the ratio of areas with positive and higher MSSS between JMA/MRI-CPS2 and the St-SCF using climate indices; (iii) AUC-av: the global average AUC; (iv) AUC-r0.5: the ratio of areas with AUC >0.5; (v) AUC-hi: the ratio of areas with AUC >0.5 and higher AUC between JMA/MRI-CPS2 and the St-SCF using climate indices. The boxes represent grids and the numbers in the boxes indicate the grid area and MSSS/AUC.

Figure 4: MSSS-rp (top) and AUC-av (bottom) by JMA/MRI-CPS2 (left: global average (GLB); center: average over land (LND); right: average over ocean (OCN)).

Figure 5: MSSS-rp (top) and AUC-av (bottom) by the St-SCF (left: global average (GLB); center: average over land (LND); right: average over ocean (OCN)).

Figure 6: Comparison of MSSS-rp (top left), MSSS-hi (top right), AUC-av (bottom left), AUC-r0.5 (bottom center), and AUC-hi (bottom right) between JMA/MRI-CPS2 and the St-SCF using climate indices.

Figure 7: Spatial distribution of MSSS for JMA/MRI-CPS2. The left, center-left, center-right, and right columns denote March, June, September, and December, respectively. The top, middle, and bottom denote the zero- to two-month leads.

Figure 8: Spatial distribution of MSSS for the St-SCF using climate indices. The left, center-left, center-right, and right columns denote March, June, September, and December, respectively. The top, middle, and bottom denote the zero- to two-month leads.

Figure 9: Climate indices selected for grids with positive MSSS. The left, center-left, center-right, and right columns denote March, June, September, and December, respectively. The top, middle, and bottom denote the zero- to two-month leads.

Figure 10: Comparison of latitude for MSSS-hi (left) and AUC-hi (right) for zero- (top) to five-month leads (bottom). The red and black lines are the values by JMA/MRI-CPS2 and the St-SCF using climate indices, respectively.

Figure 11: Comparison of precipitation at south Philippines (a; 120º E, 10º N) and southwest Australia (b; 117.5º E, 30º S) from 2001–2020 between observations (GPCP: black circle) and forecasts (red dots) by JMA/MRI-CPS2 and the St-SCF with NINO3.4 or NINO4. The MSSS values are also shown.

Figure 12: Relationship between climate indices and precipitation in south Philippines (a; 120º E, 10º N) and southwest Australia (b; 117.5º E, 30º S). The dots indicate the observational precipitation and climate indices values. The red triangles indicate the forecasted precipitation and climate indices.

Figure A1: Comparison of MSSS-rp (left) and MSSS-hi (right) between JMA/MRI-CPS2 and the St-SCF using climate indices based on the spline method (St-SCF-spl) and linear method (St-SCF-lin).

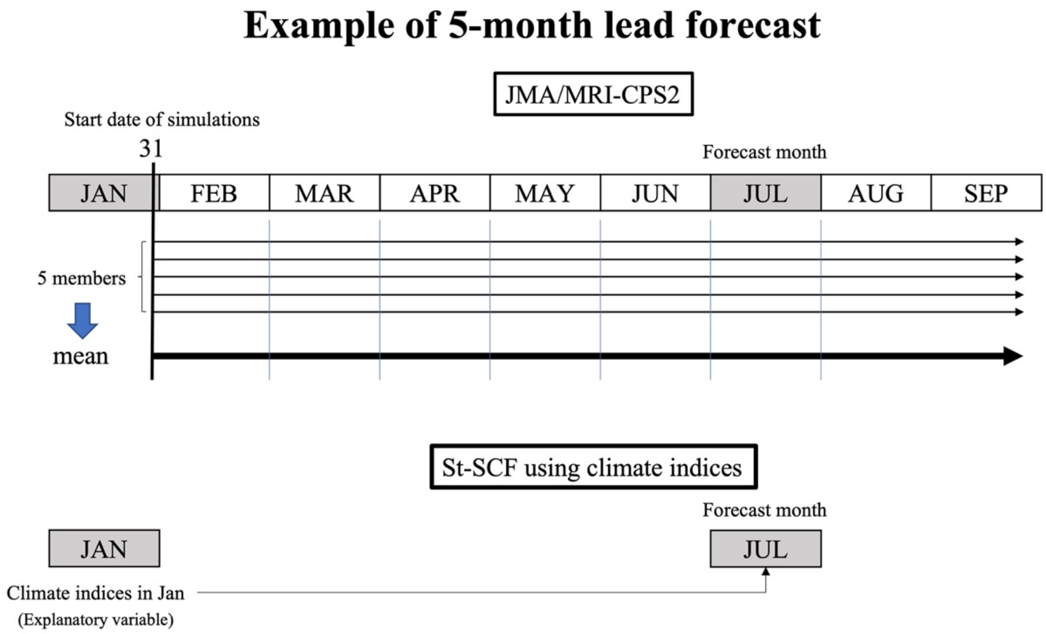

Figure 1: Five-month lead forecast by JMA/MRI-CPS2 and the St-SCF using climate indices.

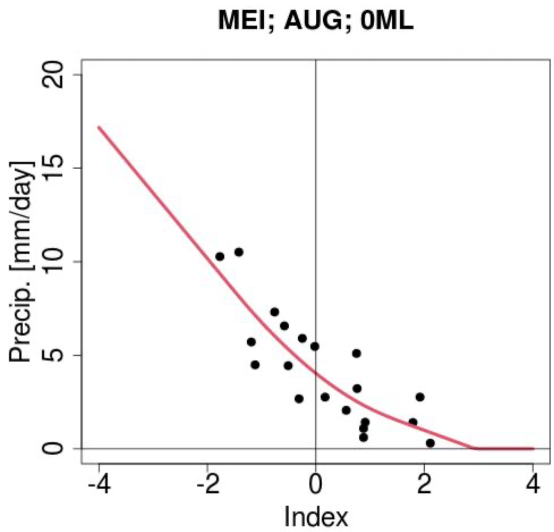

Figure 2: Spline interpolation curve (red line) of MEI in July for estimating August precipitation at 110º longitude and –2.5º latitude. The plots denote the observational precipitation and the values of the MEI.

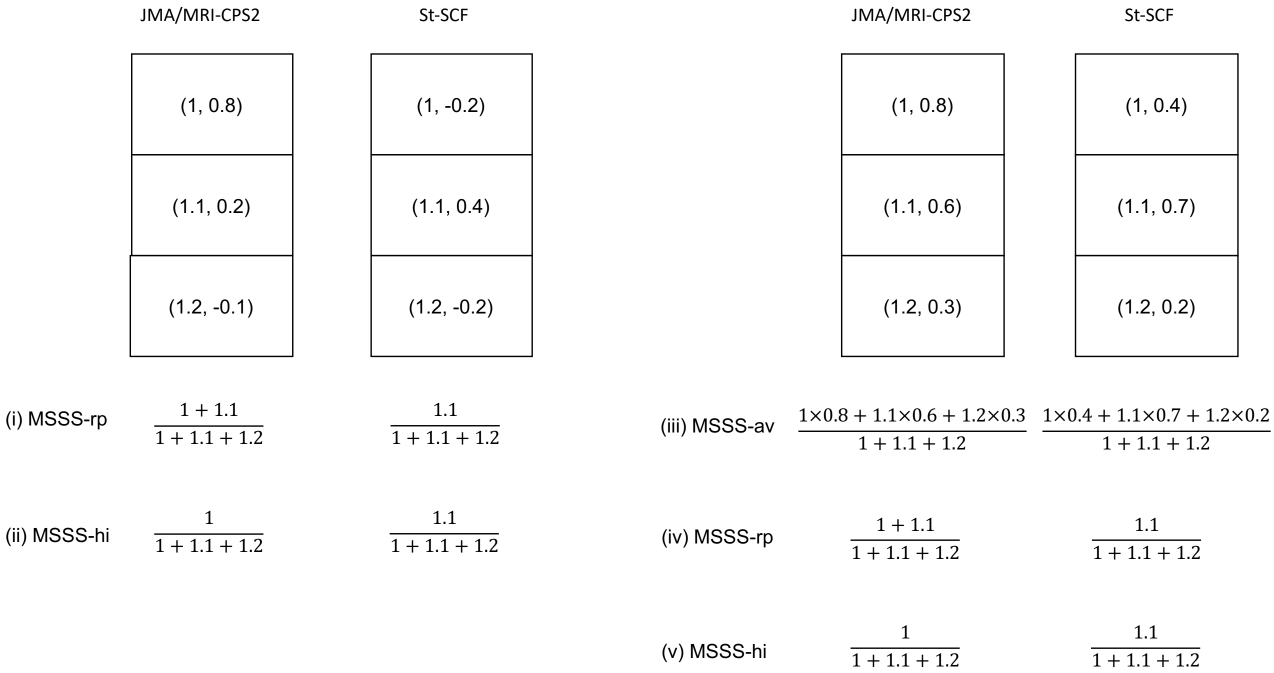

Figure 3: Example calculations of (i) MSSS-rp: the ratio of areas with positive MSSS; (ii) MSSS-hi: the ratio of areas with positive and higher MSSS between JMA/MRI-CPS2 and the St-SCF using climate indices; (iii) AUC-av: the global average AUC; (iv) AUC-r0.5: the ratio of area with AUC >0.5; (v) AUC-hi: the ratio of area with AUC >0.5 and higher AUC between JMA/MRI-CPS2 and the St-SCF using climate indices. The boxes represent grids and the numbers in the boxes indicate the grid area and MSSS/AUC.

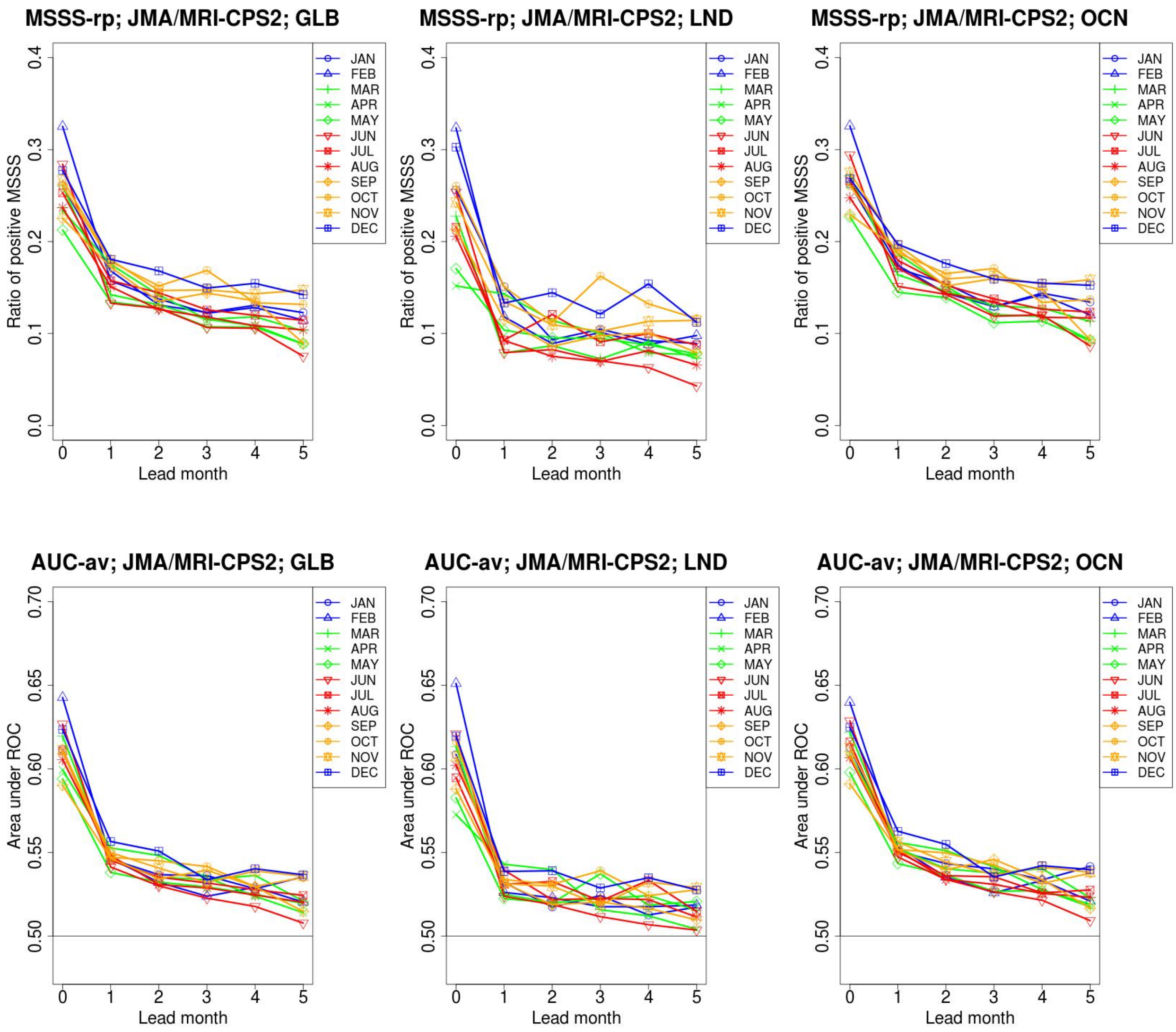

Figure 4: MSSS-rp (top) and AUC-av (bottom) by JMA/MRI-CPS2 (left: global average (GLB); center: average over land (LND); right: average over ocean (OCN)).

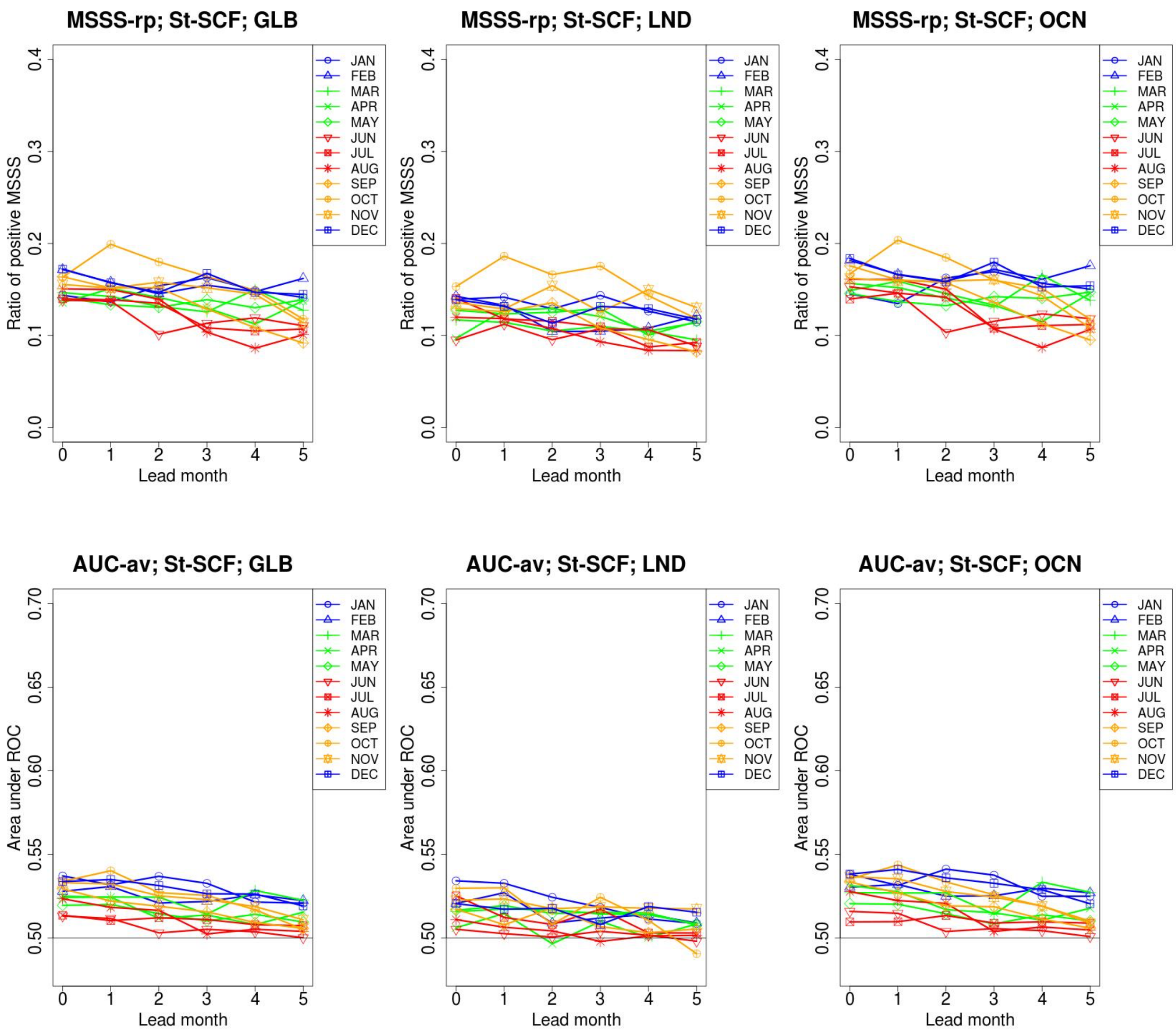

Figure 5: MSSS-rp (top) and AUC-av (bottom) by the St-SCF (left: global average (GLB); center: average over land (LND); right: average over ocean (OCN)).

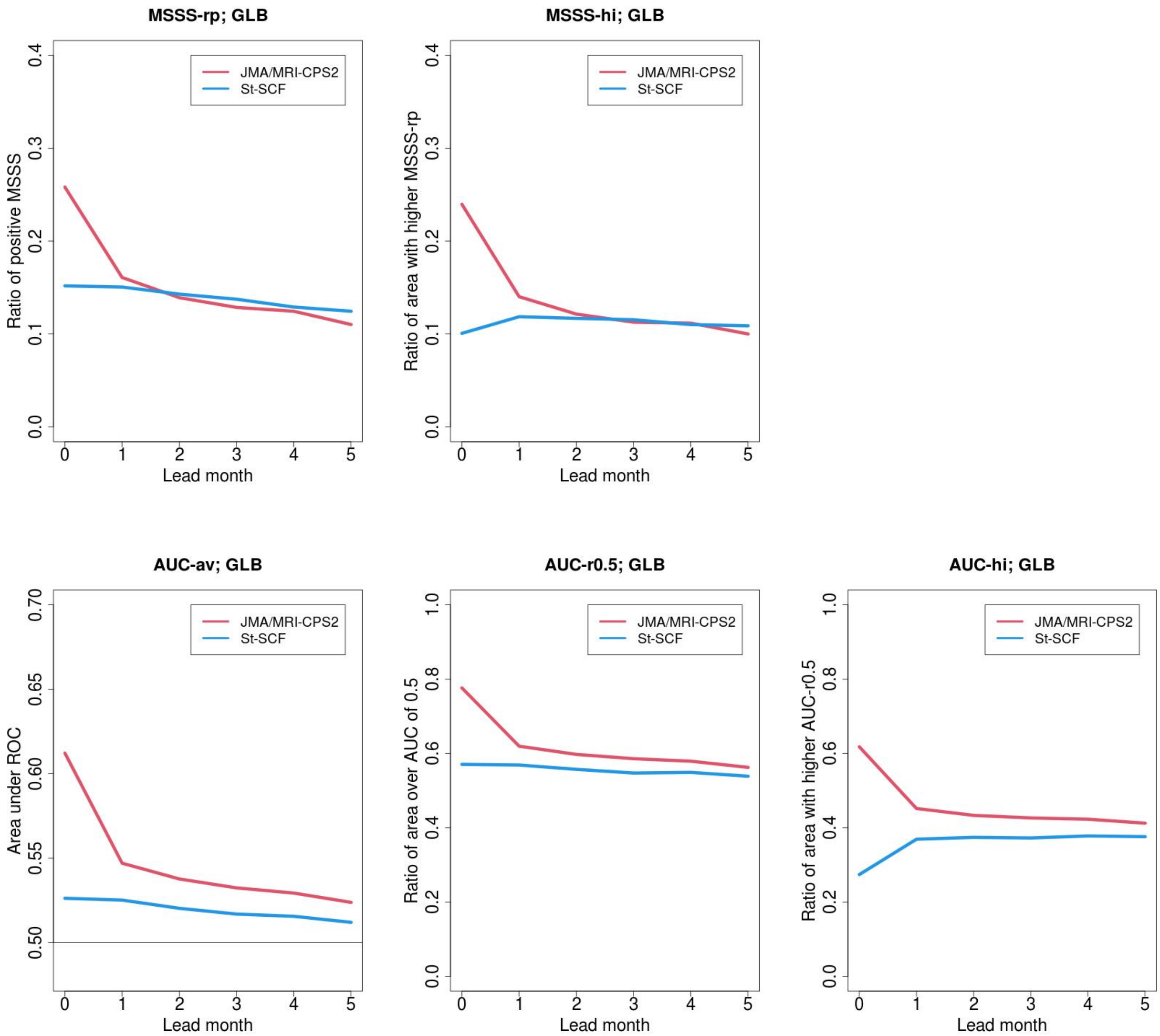

Figure 6: Comparison of MSSS-rp (top left), MSSS-hi (top right), AUC-av (bottom left), AUC-r0.5 (bottom center), and AUC-hi (bottom right) between JMA/MRI-CPS2 and the St-SCF using climate indices.

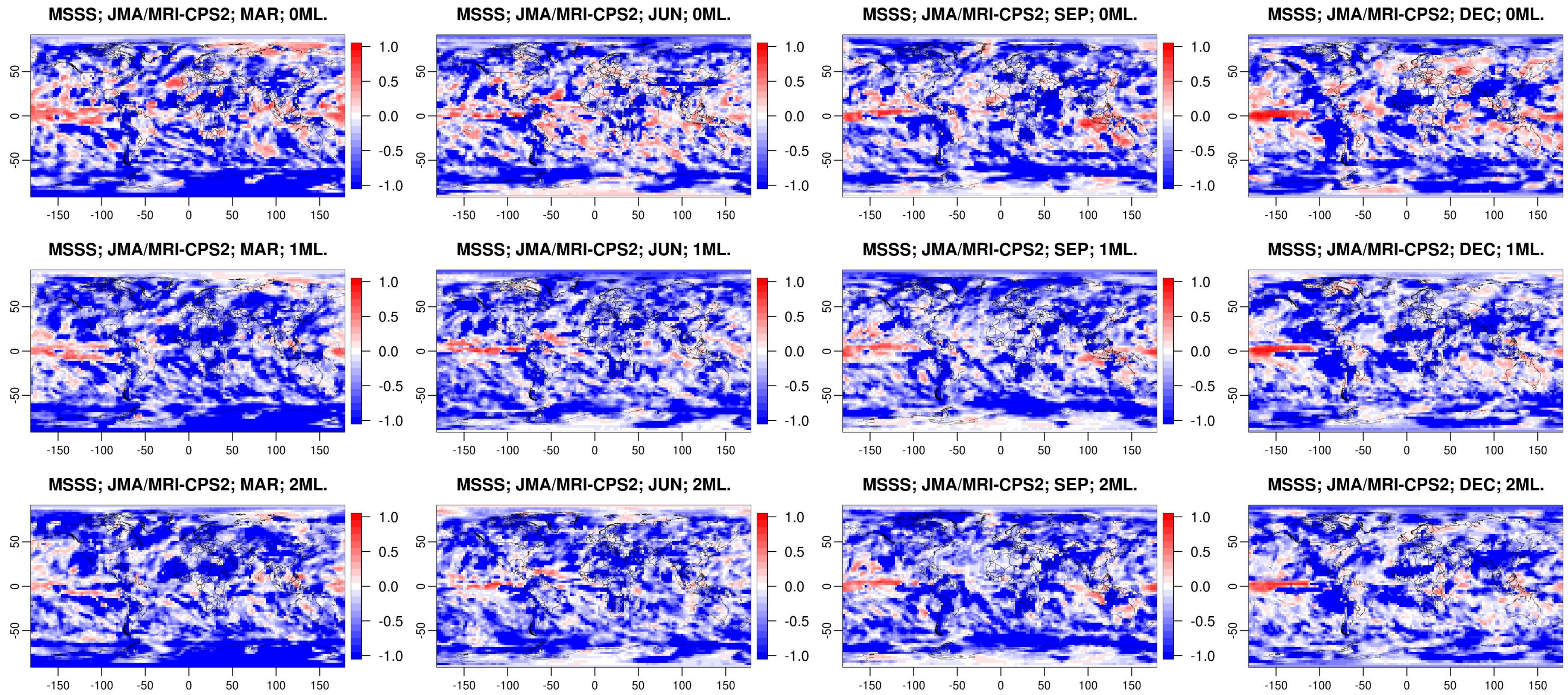

Figure 7: Spatial distribution of MSSS for JMA/MRI-CPS2. The left, center-left, center-right, and right columns denote March, June, September, and December, respectively. The top, middle, and bottom denote the zero- to two-month leads.

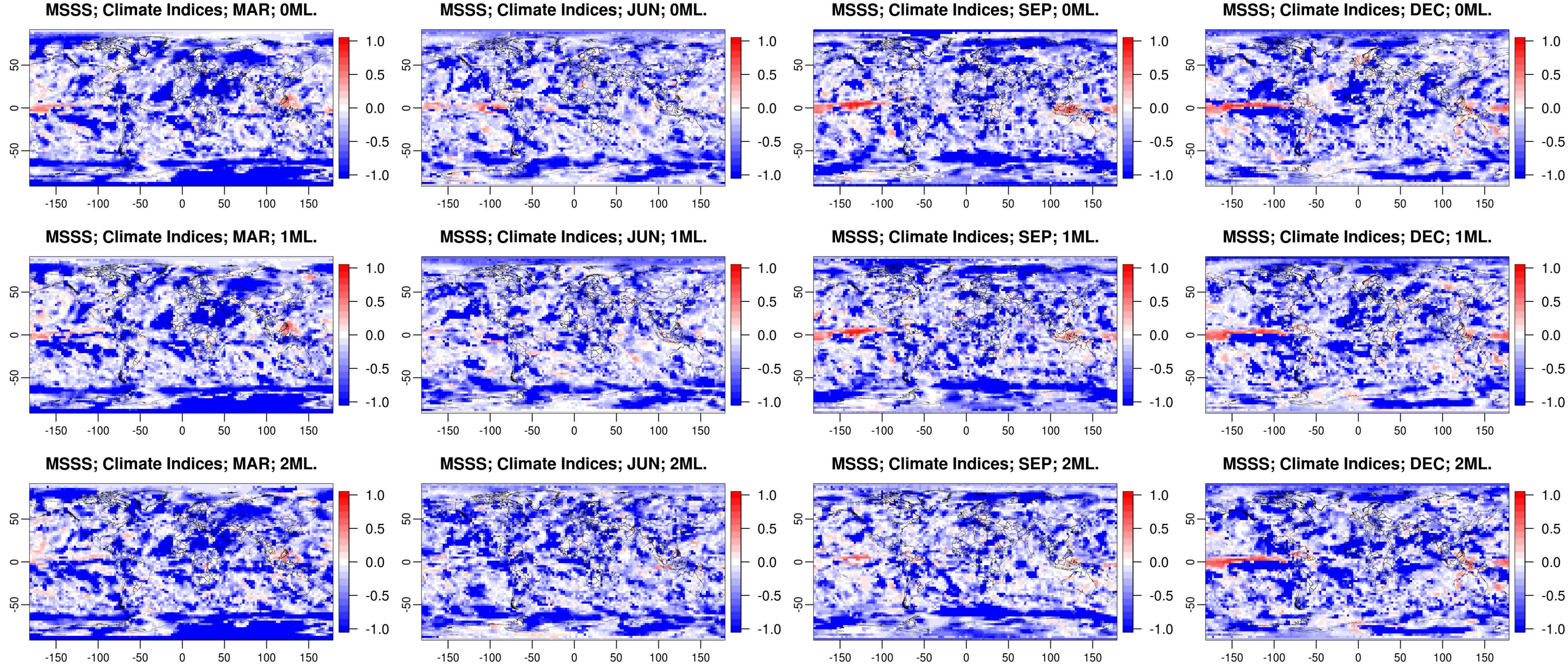

Figure 8: Spatial distribution of MSSS for the St-SCF using climate indices. The left, center-left, center-right, and right columns denote March, June, September, and December, respectively. The top, middle, and bottom denote the zero- to two-month leads.

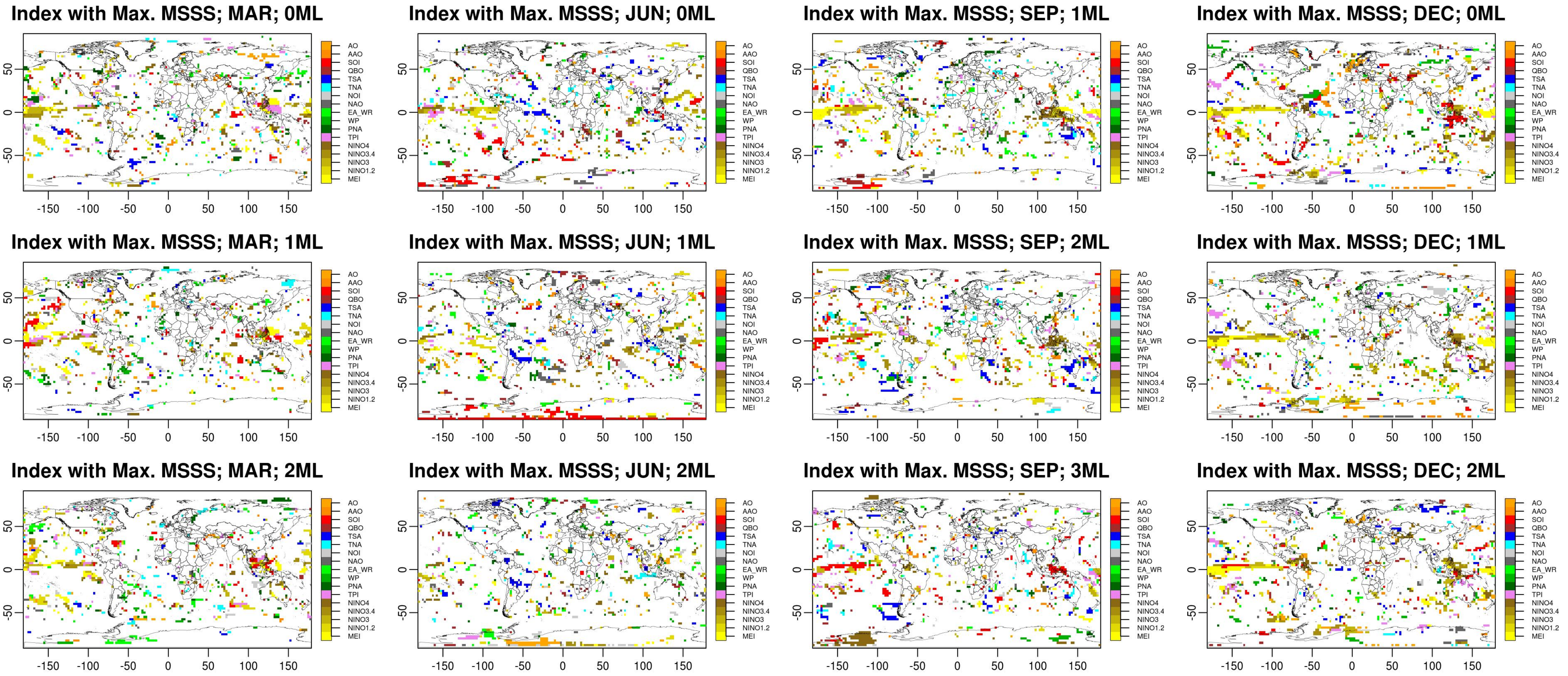

Figure 9: Climate indices selected for grids with positive MSSS. The left, center-left, center-right, and right columns denote March, June, September, and December, respectively. The top, middle, and bottom denote the zero- to two-month leads.

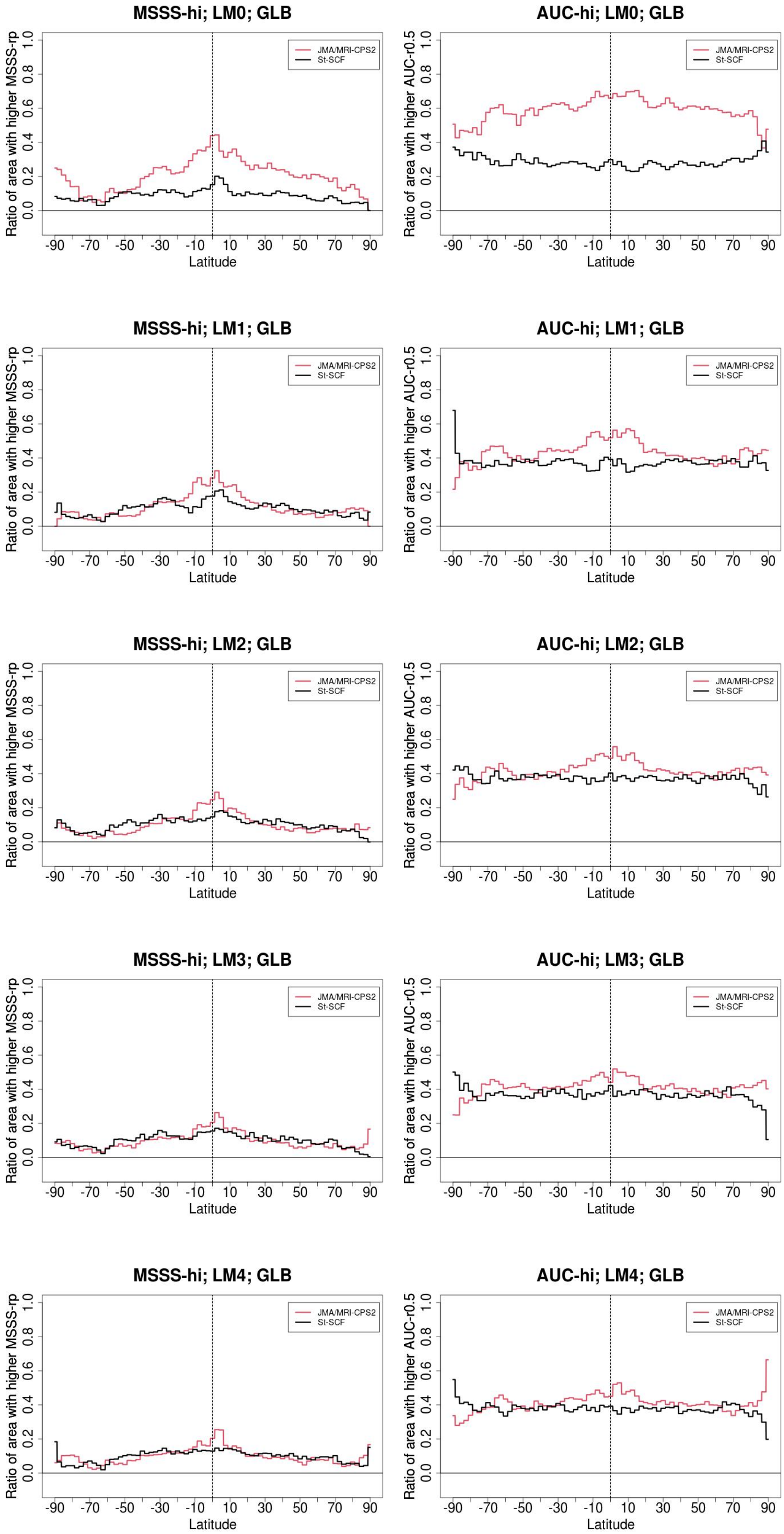
MSSS-hi; LM0; GLB
AUC-hi; LM0; GLB
MSSS-hi; LM1; GLB
AUC-hi; LM1; GLB
MSSS-hi; LM2; GLB
AUC-hi; LM2; GLB
MSSS-hi; LM3; GLB
AUC-hi; LM3; GLB
MSSS-hi; LM4; GLB
AUC-hi; LM4; GLB
JMA/MRI-CPS2
St-SCF
Ratio of area with higher MSSS-rp
Ratio of area with higher AUC-r0.5
Latitude
0.0 0.2 0.4 0.6 0.8 1.0
-90 -70 -50 -30 -10 10 30 50 70 90

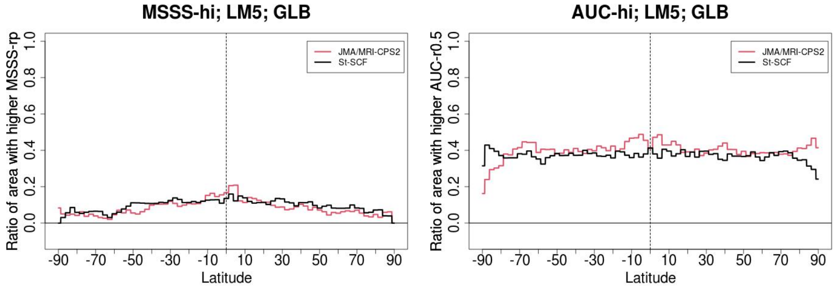

Figure 10: Comparison of latitude for MSSS-hi (left) and AUC-hi (right) for zero- (top) to five-month (bottom) leads. The red and black lines are the values by JMA/MRI-CPS2 and the St-SCF using climate indices, respectively.

(a) South Philippines

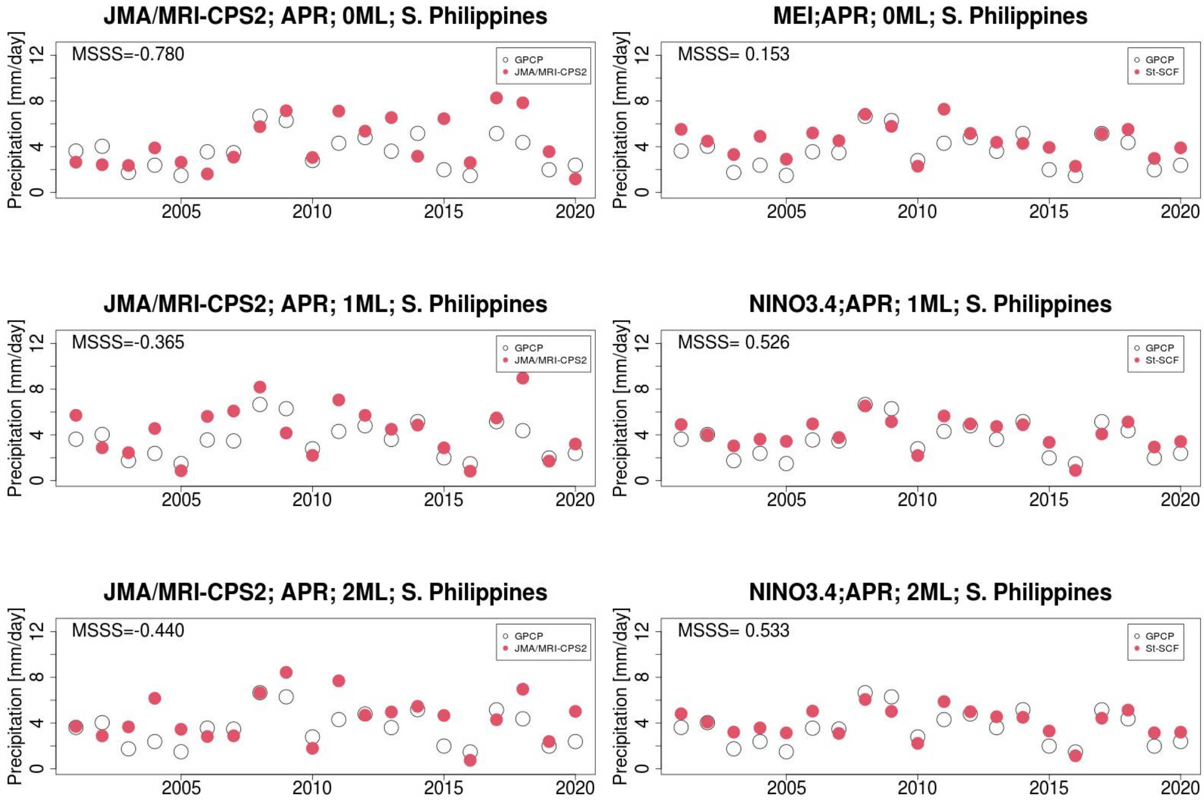

(b) Southwest Australia

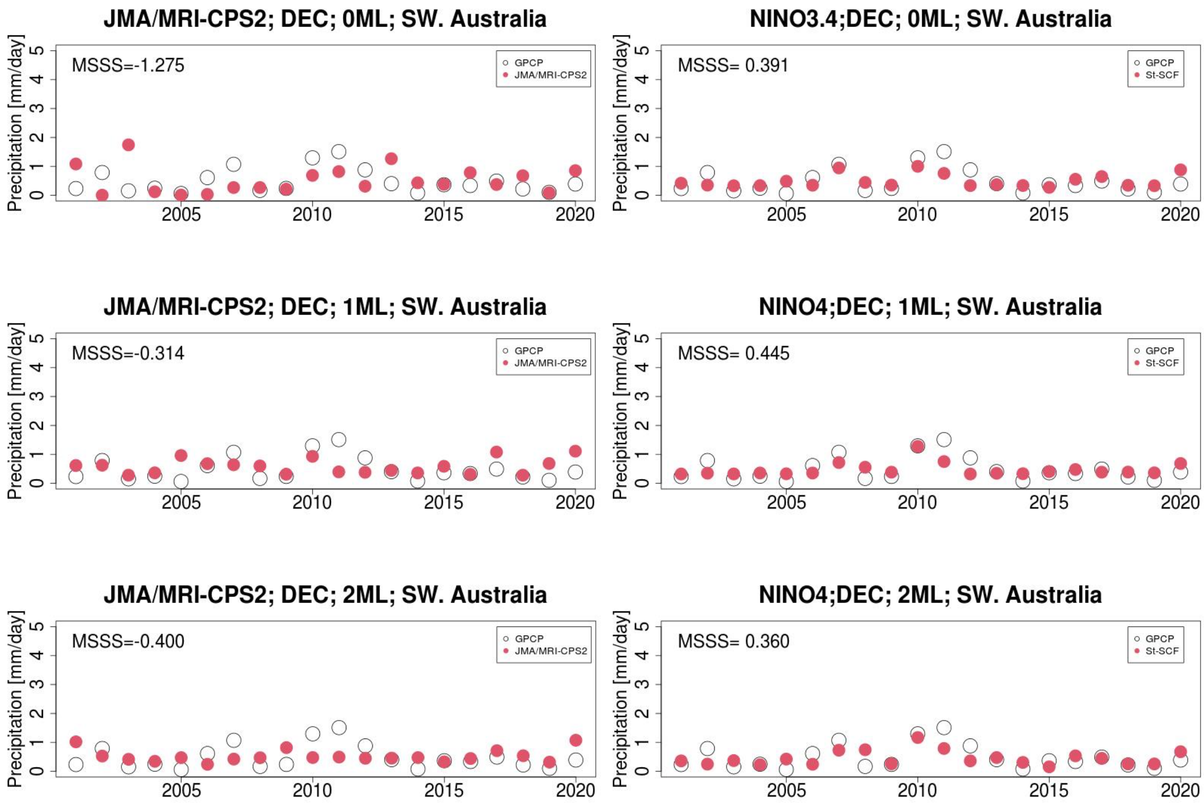

Figure 11: Comparison of precipitation at south Philippines (a; 120º E, 10º N) and southwest Australia (b; 117.5º E, 30º S) from 2001–2020 between observations (GPCP: black circle) and forecasts (red dots) by JMA/MRI-CPS2 and the St-SCF with NINO3.4 or NINO4. Ths MSSS values are also shown.

(a) South Philippines

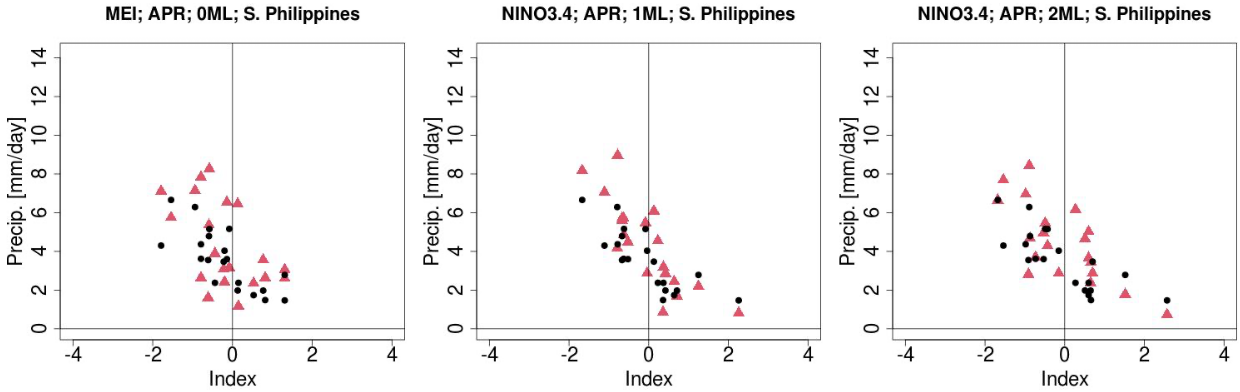

(b) Southwest Australia

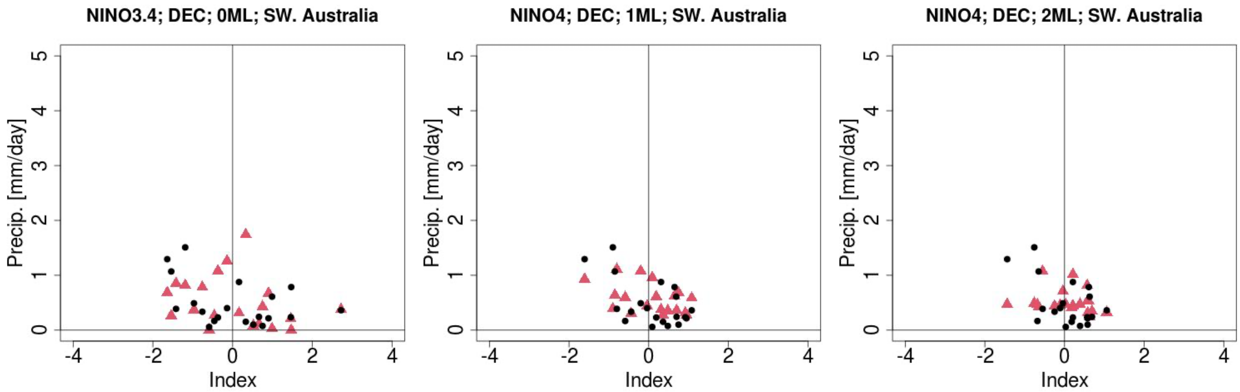

Figure 12: Relationship between climate indices and precipitation in south Philippines (a; 120º E, 10º N) and southwest Australia (b; 117.5º E, 30º S). The dots indicate the observational precipitation and climate indices values. The red triangles indicate the forecasted precipitation and climate indices values.

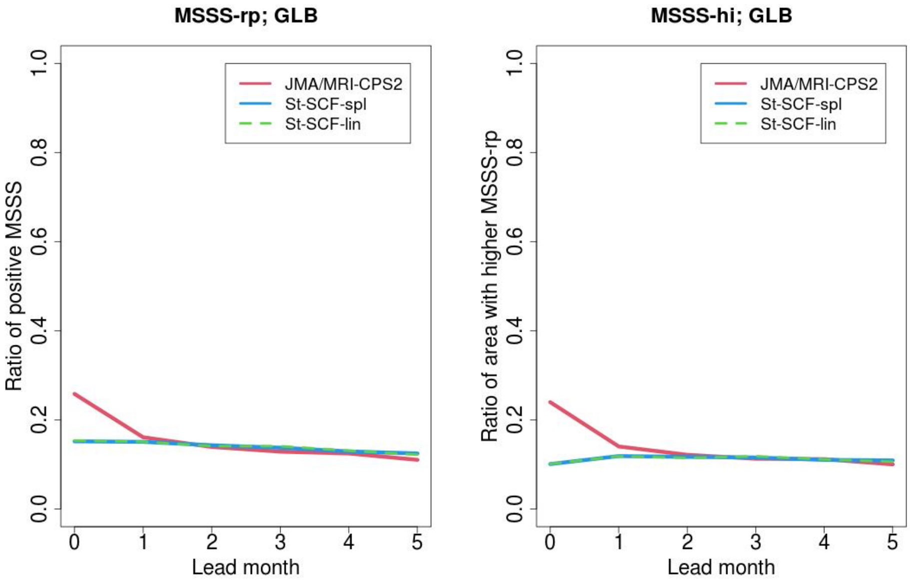

Figure A1: Comparison of MSSS-rp (left) and MSSS-hi (right), between JMA/MRI-CPS2 and the St-SCF using climate indices through the spline method (St-SCF-spl) and the linear method (St-SCF-lin).

List of Tables

Table 1: Summary of the data, models, and method used for skill evaluation.

Table 2: Seventeen climate indices evaluated in this study.

Table 3: Area ratio of selected climate indices for one-month lead forecasts.

Table 1: Summary of the data, models, and method used for skill evaluation.

Item	Description
Variable	Precipitation
Area	Global
Spatial resolution	2.5º×2.5º (144 column; 73 rows)
Period	2001–2020
Time resolution	Monthly
Lead month of prediction	0–5 months
Evaluation of forecast skill	Deterministic: Mean squared skill score (MSSS), MSSS-rp, and MSSS-hi Probabilistic: area under receiver operation characteristic curve (AUC), AUC-av, AUC-r0.5, and AUC-hi
Observation	Global Precipitation Climatology Project (GPCP) v2.3 (regrided)
Dynamical model	JMA/MRI-CPS2 (bias-corrected)
Statistical model	Seventeen climate indices

Table 2: Seventeen climate indices evaluated in this study

Category	Name	Long name	URL
Teleconnections	PNA	Pacific North American Index	ftp://ftp.cpc.ncep.noaa.gov/wd52dg/data/indices/pna_index.tim
	WP	Western Pacific Index	ftp://ftp.cpc.ncep.noaa.gov/wd52dg/data/indices/wp_index.tim
	EA/WR	Eastern Atlantic/Western Russia	ftp://ftp.cpc.ncep.noaa.gov/wd52dg/data/indices/eawr_index.tim
	NAO	North Atlantic Oscillation	ftp://ftp.cpc.ncep.noaa.gov/wd52dg/data/indices/nao_index.tim
	NOI	Northern Oscillation Index	https://www.pfeg.noaa.gov/products/PFEL/modeled/indices/NOIx/data/noix.txt
ENSO	MEI v2	Multivariate ENSO Index	https://psl.noaa.gov/enso/mei/data/meiv2.data
	Nino 1+2	Extreme Eastern Tropical Pacific SST (0-10S, 90W-80W)	http://www.cpc.ncep.noaa.gov/data/indices/ersst5.nino.mth.91-20.ascii
	Nino 3	Eastern Tropical Pacific SST (5N-5S, 150W-90W)	http://www.cpc.ncep.noaa.gov/data/indices/ersst5.nino.mth.91-20.ascii

	Nino 4	**Central Tropical Pacific SST (5N-5S) (160E-150W)**	**http://www.cpc.ncep.noaa.gov/data/indices/ersst5.nino.mth.91-20.ascii**
	Nino 3.4	**East Central Tropical Pacific SST (5N-5S) (170-120W)**	**http://www.cpc.ncep.noaa.gov/data/indices/ersst5.nino.mth.91-20.ascii**
SST: Pacific (except ENSO)	**TPI(IPO)**	**Tripole Index for the Interdecadal Pacific Oscillation (unfiltered)**	**https://psl.noaa.gov/data/timeseries/IPOTPI/tpi.timeseries.ersstv5.data**
SST: Atlantic (except WHWP)	**TNA**	**Tropical Northern Atlantic Index**	**https://www.esrl.noaa.gov/psd/data/correlation/tna.data**
	TSA	**Tropical Southern Atlantic Index**	**https://www.esrl.noaa.gov/psd/data/correlation/tsa.data**
Atmosphere	**QBO**	**Quasi-Biennial Oscillation**	**https://www.esrl.noaa.gov/psd/data/correlation/qbo.data**
	SOI	**Southern Oscillation Index**	**https://www.esrl.noaa.gov/psd/data/correlation/soi.data**
	AAO	**Antarctic Oscillation**	**http://www.cpc.ncep.noaa.gov/products/precip/CWlink/daily_ao_index/aa**

		o/monthly.aao.index.b79.current.ascii
AO	Antarctic Oscillation	http://www.cpc.ncep.noaa.gov/products/precip/CWlink/daily_ao_index/monthly.ao.index.b50.current.ascii

Table 3: Area ratio of selected climate indices for one-month lead forecasts.

Climate Index	Area ratio
MEI	0.0161
NINO1.2	0.0123
NINO3	0.0125
NINO3.4	0.0120
NINO4	0.0127
TPI	0.0091
PNA	0.0069
WP	0.0068
EA_WR	0.0058
NAO	0.0054
NOI	0.0071
TNA	0.0054
TSA	0.0093
QBO	0.0048
SOI	0.0133
AAO	0.0063
AO	0.0059